In-situ non-contact monitoring algorithm for PET crystallinity and moisture content using Terahertz time-domain spectroscopy

Sang-Il Kim [a], Dong-Woon Park [a], Heon-Su Kim [a], Hak-Sung Kim [a,b,*]

[a] *Department of Mechanical Convergence Engineering, Hanyang University, 222, Wangsimni-ro, Seongdong-gu, Seoul, Republic of Korea*
[b] *Institute of Nano Science and Technology, Hanyang University, 222, Wangsimni-ro, Seongdong-gu, Seoul, Republic of Korea*

ARTICLE INFO

ABSTRACT

A terahertz time-domain spectroscopy (THz-TDS) system was used to monitor the crystallinity and moisture content of polyethylene terephthalate (PET) specimens. The crystallinity and moisture content were varied by controlling cooling rate and immersion time. Crystallinity, crystallite size, and moisture content of the PET specimens were measured through differential scanning calorimetry (DSC), x-ray diffraction (XRD), and gravimetric methods, respectively. The THz signal with regard to crystallinity and moisture content was subsequently analyzed within the time and frequency-domain. In addition, optical properties of refractive index and absorption coefficient were derived. Consequently, the crystallinity and moisture content could be simultaneously measured by analyzing the THz signals.

1. Introduction

Polyethylene terephthalate (PET), a thermoplastic with high strength, chemical resistance, and formability, has been used in a variety of industries including electronics, construction, and packaging [1–4]. The mechanical properties of PET are affected by crystallinity and moisture content as the polymer chains are changed during manufacturing [5,6]. As the degree of PET crystallinity increases, the polymer chain and density are increased, resulting in an enhancement of toughness and strength but a reduction in impact strength due to brittleness [5]. Furthermore, moisture absorption can lead to hydrolysis reactions that break polymer chains, resulting in reduction in elastic modulus and strength [7,8]. Therefore, to ensure the reliability of PET components, a proper degree of crystallinity and moisture content must be controlled during manufacturing processes and should be monitored during its service duration.

Generally, the crystallinity of a polymer product is analyzed via differential scanning calorimeter (DSC) and X-ray diffraction (XRD) techniques [9,10]. However, these techniques each have their own limitations. DSC can calculate crystallinity by measuring enthalpy during heating or cooling. However, it is not an *in situ* technique as a small piece of the specimen should be melted or burned during the test. XRD measures the crystal structure of a specimen by measuring the diffraction generated after X-ray irradiation. XRD uses high energy X-rays, which are hazardous to the human body. XRD also is not a real-time inspection because the sample should be placed on a table to precisely control the X-ray incident angle. In addition, this method requires a long measurement time as X-rays are scanned at various angles and the reflected X-rays are analyzed.

To monitor the moisture content absorbed in the materials, electrical conductivity and gravimetric methods have been used widely [11,12]. However, the former can only measure the moisture content on the surface of the specimen. In addition, it measures the moisture content with a low resolution at the beginning of moisture absorption. This is because the polymer material takes a long time to change conductivity after absorbing moisture [12]. The gravimetric method periodically measures the weight of a specimen with absorbed moisture and can measure the moisture content more precisely than the former method. Nevertheless, it is also not an *in-situ* measurement technique.

There are various types of *in-situ* measurement techniques, such as thermography, optical spectroscopy, and terahertz spectroscopy. Thermography is effective in detecting hot objects or objects with strong heat emissions, and it can be relatively simple and cost-effective to set up with less sophisticated equipment [13]. However, this technique has a thermal deformation issue of the specimen because it requires applying heat to the measurement specimen [14]. Optical spectroscopy provides high spatial resolution and real-time detection by detecting changes in the optical properties of materials, and it is sensitive to material

characteristics [15]. Nevertheless, it has limitations in detecting inside materials due to the low penetration [16].

In comparison, terahertz spectroscopy offers higher resolution analysis than thermography and higher penetration depth than optical spectroscopy [17]. Therefore, terahertz spectroscopy has gained significant attention in recent years due to its unique capabilities for material analysis in fields such as material science, biomedical imaging, and security screening [17]. However, terahertz spectroscopy has limitations in penetrating materials that contain metals [18].

Several studies have been conducted to investigate the crystallinity of polymer materials using THz spectroscopy. Stefan Sommer conducted research on the evaluation of crystallinity in high-density polyethylene (PE-HD) using THz spectroscopy with complex permittivity and refractive index [19]. Han Wang examined the crystallinity of cellulose using THz mass absorption coefficients [20]. In addition, Francisco Senna Vieira investigated cellulose crystallinity using the THz-TDS system and the standard normal variate algorithm (SNV) to standardize the data [21]. Crystallinity analysis was performed on food items such as corn and potatoes using THz spectral absorbance by Shusaku Nakajima [22]. Previous studies primarily focused on the analysis of material crystallinity. However, it is important to consider that polymer materials are influenced not only by crystallinity but also by moisture content. Therefore, the simultaneous assessment of both the crystallinity and moisture content of polymer materials is essential for real-world products.

In this work, a pulsed THz inspection technique was used to detect and analyze the characteristics (crystallinity and moisture content) of a PET product in real-time. THz waves are electromagnetic with a frequency range between 0.1 THz and 10 THz. THz waves can be used to inspect products without deterioration due to their low energy [23,24], and they are safe for the human body. In addition, THz waves can inspect materials in real-time without any additional medium due to their linearity in air [23]. THz waves are especially sensitive to the crystal structure and moisture content in a polymer due to scattering and absorption by water molecules [25].

Therefore, in this study, the degree of crystallinity and moisture content of PET specimens were analyzed using a THz-TDS system (Fig. 1). The crystallinity and moisture content of PET specimens were varied by controlling the cooling rate and immersion time in water, respectively. The THz signals with respect to crystallinity and moisture content were measured in transmission and transformed into a frequency spectrum via fast Fourier transformation (FFT). Then, the relationships between the PET properties and THz signal were analyzed by extracting several THz parameters such as peak amplitude and index over the time and frequency-domain. These results also were compared to those measured by DSC, XRD, and gravimetric techniques. Optical

properties of refractive index and absorption coefficient of the PET specimen were also investigated.

2. Experiment

2.1. Sample preparation

The PET specimens were fabricated according to ASTM D 570 [11]. A total of 22 films of PET (SKC Co., South Korea) each with a thickness of 50 μm was stacked and molded at 0.2 MPa and 300 °C for 3 min using a hot-press, as shown in Fig. 2-(a). The thickness of the specimen was controlled at 1.0 mm. The degree of PET crystallinity of the specimens was controlled by the cooling rate. The specimens were cooled at three rates: fast-cooling (quenching) (100 °C/min), normal-cooling (normalizing) (13 °C/min), and slow-cooling (annealing) (2 °C/min) as shown in Fig. 2-(b), (c), and (d), respectively. Fast-cooling was performed by ice-water quenching (Fig. 2-(b)), normal-cooling was performed using a water-chilled mold (Fig. 2-(c)), and slow-cooling was performed by air convection (Fig. 2-(d)). To evaluate the reproducibility of the experiments, three PET specimens were prepared for each cooling rate, and three measurements were taken per specimen using THz waves.

After 24 h of desiccation, PET specimens with different moisture contents were prepared via water immersion as shown in Fig. 3. The specimens were immersed in distilled water at room temperature, and their weight was periodically measured using an electronic scale based on ASTM D 570 [11] (20 min, 40 min, 60 min, 2 h, 24 h, 2 days, and 13 days).

2.2. THz inspection system

A THz-TDS system, FiCO™ (Zomega Corporation, NY, USA) was used to analyze the degree of crystallinity and moisture content of the PET specimens as shown in Fig. 4. The system was composed of a femtosecond laser, a pair of THz modules, and optical instruments (Fig. 4-(a)). The system exhibited a frequency range between 0.1 and 3.0 THz, a frequency resolution of 11 GHz, a time resolution of 20 fs, and a signal-to-noise ratio (SNR) of 60 dB. The THz system was set up in transmission mode (Fig. 4-(b)), in which the THz modules were coaxially aligned with the specimen. To avoid THz wave absorption by moisture, the relative humidity was kept below 5% using dry air [25]. The temperature was maintained at room temperature.

2.3. Characterization of the PET specimens

DSC (SDT Q600, Auto-DSCQ20 System, TA Instruments, USA) was used to measure the crystallinity of the PET specimens. The heating rate
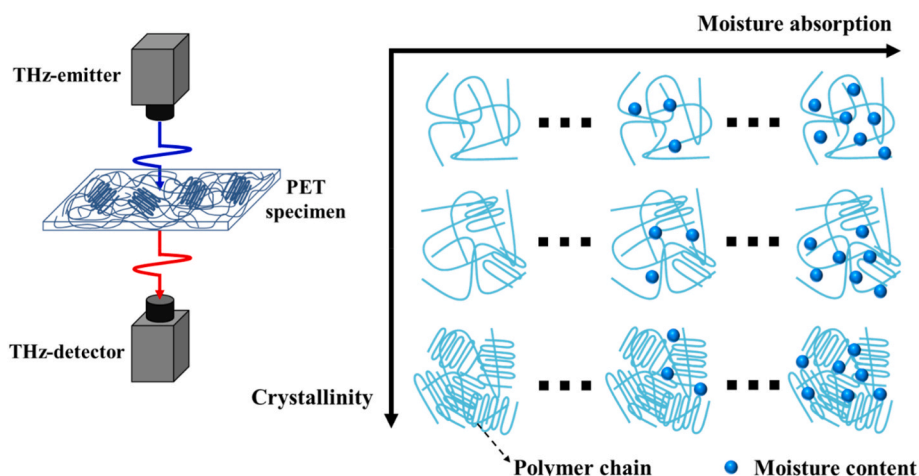

Fig. 1. Schematic representation of the in-situ non-contact monitoring algorithm for the crystallinity and moisture content of the PET using the THz-TDS system.
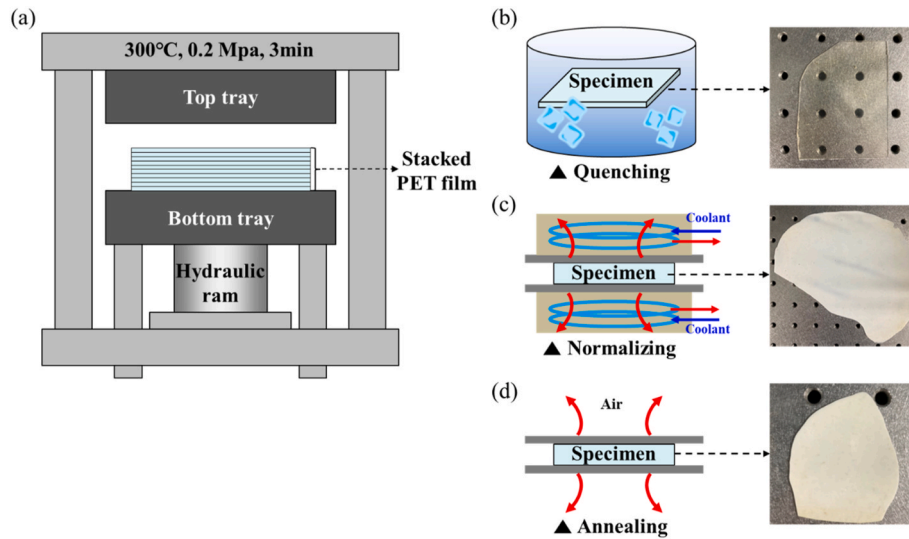
Fig. 2. Schematic representation of the manufacturing process of the PET specimens: (a) hot press molding process, (b) fast-cooling (quenching), (c) normal-cooling (normalizing), and (d) slow-cooling (annealing).
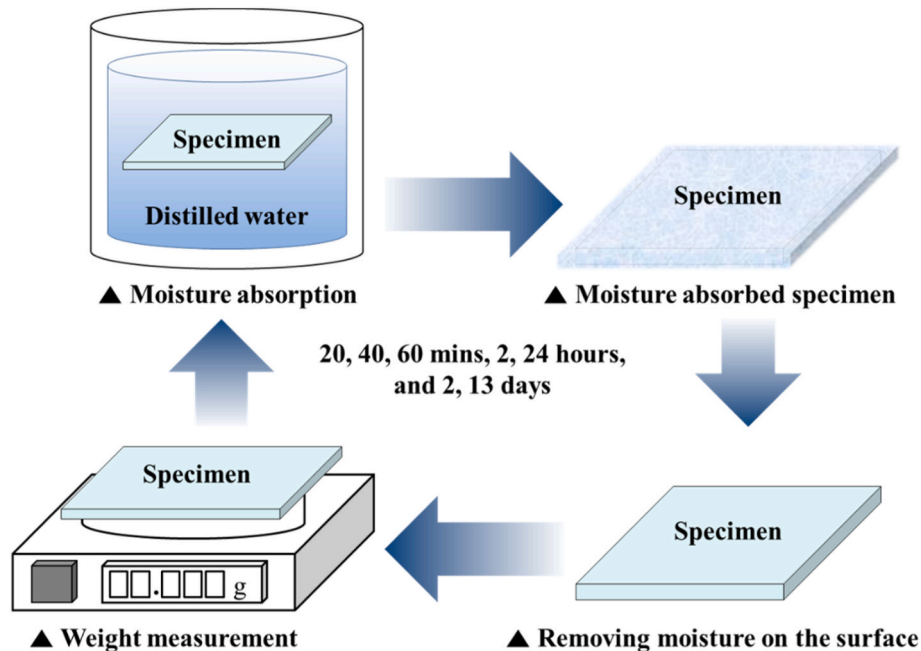

Fig. 3. Schematic representation of the moisture absorption test of the PET specimens.

was set to 10 °C/min from 25 °C to 297 °C. The degree of crystallinity (K_{DSC}) was calculated as follows:

$$\Delta H_m(T_2) - \Delta H_m(T_1) = \int \Delta C_p dT \qquad (1)$$

$$K_{DSC} = \frac{\Delta H_m - \Delta H_c}{\Delta H_{lit}} \qquad (2)$$

where ΔH_m, ΔH_c, and ΔH_{lit} are the melting enthalpy, crystallization enthalpy, and enthalpy of melting for 100% crystallinity (140 J/g), respectively [10].

Furthermore, the degree of crystallinity (K_{XRD}) and crystallite size (D_c) were measured using XRD (XRD, D8 ADVANCE, Bruker, USA) with Cu-K (=1.5418). The analysis angle was varied from 10° to 45° and the scan speed was set to 1 s. The degree of crystallinity was calculated using

Eq. (3) [10]:

$$K_{XRD} = \frac{A_{cry}}{A_{cry} + A_{amo}} \qquad (3)$$

where A_{cry} and A_{amo} are the intensity area of the crystalline phase and amorphous phase, respectively. In addition, the crystallite size (D_c) of the PET specimen was calculated using Eq. (4):

$$D_c = \frac{e \bullet \lambda}{\beta \bullet \cos(\theta)} \qquad (4)$$

where e, λ, β, and θ are the shape factor, X-ray wavelength, peak half value, and Bragg angle, respectively.

With regard to moisture content, a gravimetric method was used with an electronic scale. The moisture content of the PET specimen was calculated using Eq. (5):
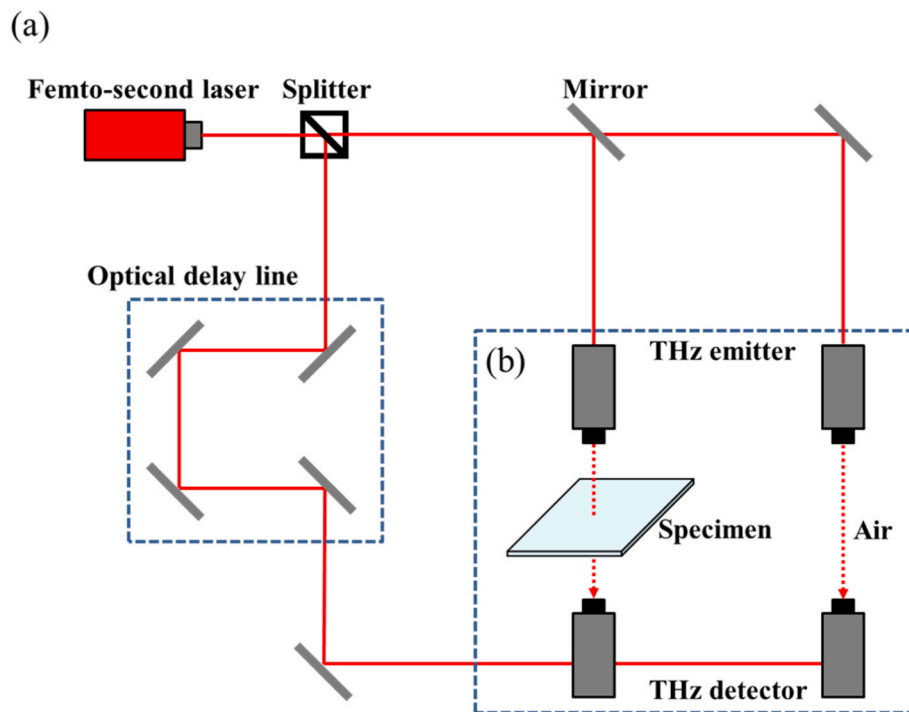
Fig. 4. Schematic representation of the THz-time domain spectroscopy (THz-TDS): (a) overall system, and (b) transmission mode diagram.

$$\text{water content } (\%) = \frac{m_{wet} - m_{dry}}{m_{dry}} \qquad (5)$$

where m_{wet} is the weight of the PET specimen during moisture absorption, and m_{dry} is the weight when fully dried.

3. Results and discussion

3.1. Degree of crystallinity and moisture content inspection using conventional methods

DSC and XRD experiments were conducted to measure the degree of crystallinity of the PET specimens. Fig. 5-(a) shows the heat flow history of the PET specimens from the DSC. The polymer chain structure of the fast-cooled (quenched) specimen recrystallized during heating from an amorphous state. Therefore, glass transition and cold crystallization peaks were detected near 75 °C and 123.7 °C, respectively, in the fast-cooled specimen. Glass transition and cold crystallization peaks were not found in the heat flow histories of the normal (normalized) and slow-cooled (annealed) specimens. All endothermic peaks due to PET specimen melting were detected between 254 and 258 °C, which confirmed

complete melting during manufacturing at 300 °C.

Table 1 shows the degree of crystallinity with regard to the cooling rate calculated from the heat flow history based on Eq. (2). As the cooling rate increased, crystallinity decreased since the higher cooling rate prevented the formation of polymer crystal structures [10,26].

XRD was performed to confirm the degree of crystallinity and the crystallite sizes of the PET specimens according to the cooling rate. Fig. 5-(b) shows the diffraction intensity of the x-ray-irradiated specimens as a function of incident angle. The XRD peaks were not detected in the quenched specimen due to their amorphous nature, resulting in the absence of distinct crystalline planes during the fast-cooling process.

Table 1
PET specimen crystallinity analyzed by DSC and XRD.

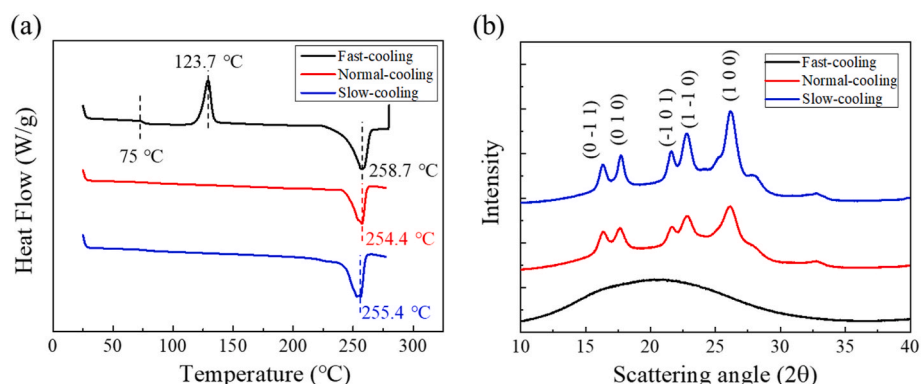| Specimens	DSC	XRD	
Cooling rate [°C/ min]	Crystallinity [%]	Crystallinity [%]	Crystallite size [nm]
100	14.3	–	–
13	34.2	38.7	95
2	41.4	45.8	200

Fig. 5. PET characteristic inspection according to the cooling rate in the manufacturing process: (a) DSC, and (b) XRD.

However, as the crystallinity increased due to the use of normal-cooling and slow-cooling rates, distinct XRD intensity peaks were observed at specific scattering angles (2θ), including 16.1°, 17.4°, 21.6°, 22.7°, and 26.0°, which correspond to (0 -1 1), (0 1 0), (−1 0 1), (1 -1 0), and (1 0 0) crystal planes, respectively. The crystalline peak intensity in the XRD of PET specimens was observed to increase as the cooling rate decreased. The observed phenomenon can be attributed to an increase in the crystalline region of the PET specimen resulting from a lower cooling rate. This lower rate of cooling promotes greater alignment of crystals in the amorphous region, thereby increasing the reflection of X-rays by larger crystal planes. Moreover, the reduction in amorphous regions results in decreased absorption of X-rays by the specimen.

The scattering angles (2θ) of the crystalline peaks of the normal and slow-cooled specimens were used to calculate the degree of crystallinity and crystallite sizes using Eqs. (3) and (4); the results are summarized in Table 1. The crystallinity and crystallite sizes of the specimens measured via XRD decreased as the cooling rate increased, and the level of crystallinity was similar to that from the DSC experiments. However, in the fast-cooled specimen, the crystallinity and crystallite sizes could not be calculated due to the smooth curve of the amorphous state of the specimen.

The moisture content of the PET specimens during moisture absorption was periodically monitored via gravimetric measurement at 20, 40, 60 min, 2, 24 h, and 2, 13 days (Fig. 3). Fig. 6 shows the moisture content of the specimens with different levels of crystallinity with regard to immersion time. The moisture content was saturated after 2 days of immersion, and the saturation moisture weight increased as the degree of crystallinity decreased. This was because the specimen permeability increased as the PET became amorphous. Also, water permeability through the polymer decreased as the density of the polymer specimen increased (more crystallized) [27].

3.2. Degree of crystallinity and moisture content inspection using THz waves

3.2.1. THz wave parameters

Fig. 7-(a) and (b) show the time-domain and frequency-domain THz signals, which were periodically measured during immersion of the specimens. The amplitude of the signal in the time-domain and frequency-domain of the THz waves decreased according to immersion time. This was because moisture could absorb THz electromagnetic waves over the entire THz frequency range [28]. To compare the THz
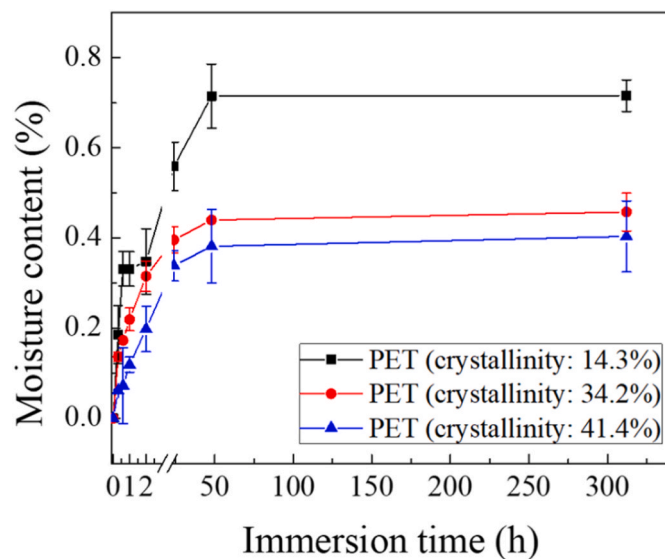

Fig. 6. Moisture content of the PET specimen during moisture absorption with different crystallinity.

absorption rate according to immersion time, the THz amplitude ratio ($\widetilde{E}_{amp\ ratio}$) was defined using Eq. (6):

$$\widetilde{E}_{amp\ ratio} = \frac{\widetilde{E}_t}{\widetilde{E}_0} \tag{6}$$

where $\widetilde{E}_t$ and $\widetilde{E}_0$ are the THz amplitudes at a frequency of 0.86 THz during immersion time t and prior to immersion (dry state), respectively. From Fig. 7-(b), a signal with a high signal-to-noise ratio (SNR) greater than 50 dB was found in the 0.43 to 0.86 THz range. In particular, the THz amplitude at a frequency of 0.86 THz was sensitively reduced due to moisture absorption after water molecule rotation [29]. Therefore, an amplitude of 0.86 THz was chosen to inspect the degree of PET moisture absorption with high resolution. The THz amplitude ratio ($\widetilde{E}_{amp\ ratio}$) decreased rapidly until 2 days after immersion, when the film was saturated (Fig. 9-(a)).

The crystallinity of the PET specimens was difficult to distinguish as the water molecules influenced the signal across the entire THz bandwidth. On the other hand, scattering due to crystallinity differed by THz frequency range as shown in Fig. 7-(b). Amorphous PET with a lower crystallinity better absorbed high frequency THz waves than low frequencies regardless of moisture absorption, showing an inclined frequency-domain signal (see left side of Fig. 7-(b)). Meanwhile, as the crystallinity of the PET specimen increased, the frequency-domain THz wave flattened (see middle and right in Fig. 7-(b)). This tendency became more obvious in Fig. 8-(a), where the frequency-domain THz wave amplitude of the dry PET specimens with different degrees of crystallinity were plotted together. The amplitude ratios of the low and high frequencies differed by crystallinity of the PET specimens. This coincided with the report of Hong et al. that electromagnetic waves were shifted from low to high frequencies by scattering as crystallite size decreased [30]. In the amorphous PET specimen with low crystallinity and small crystallite size, the high frequency region of the THz wave was scattered, while low frequency THz waves penetrated the PET specimen. On the other hand, in the PET specimens with high crystallinity and large crystallite sizes, the low frequency region of the THz wave was scattered, while the waves in the high frequency region penetrated the PET specimen (Fig. 8-(b)).

To distinguish the degree of crystallinity along with the moisture absorption of the PET specimen, the ratio ($\widetilde{E}_{low\ to\ high}$) of THz amplitude at high and low frequencies was utilized and defined by Eq. (7):

$$\widetilde{E}_{low\ to\ high} = \frac{\widetilde{E}_{low}}{\widetilde{E}_{high}} \tag{7}$$

where $\widetilde{E}_{low}$ and $\widetilde{E}_{high}$ are the amplitudes of the signal at low and high frequencies, respectively. To select low and high frequencies, the difference in THz amplitude according to the crystallinity was analyzed in the frequency domain using Eq. (8):

$$Difference = \left| \widetilde{E}_{14.3\%} - \widetilde{E}_{41.4\%} \right| \tag{8}$$

where $\widetilde{E}_{14.3\%}$ and $\widetilde{E}_{41.4\%}$ are the THz amplitudes of the PET specimens with the crystallinities of 14.3% and 41.4%, respectively. The difference in the THz amplitude according to the crystallinity of the PET specimen was increased from 0.43 THz and maximized at 0.86 THz (Fig. 8-(c)). Therefore, low and high frequencies were selected for 0.43 THz and 0.86 THz, respectively. When measuring different types of specimens, it is necessary to calibrate the frequency range using Eq. (8) because the frequency range for the low/high amplitude ratios varies depending on the thickness and type of the sample.

The THz amplitude ratios between the high and low frequency regions ($\widetilde{E}_{low\ to\ high}$) were plotted in Fig. 9-(b) with respect to PET specimen crystallinity during moisture absorption.
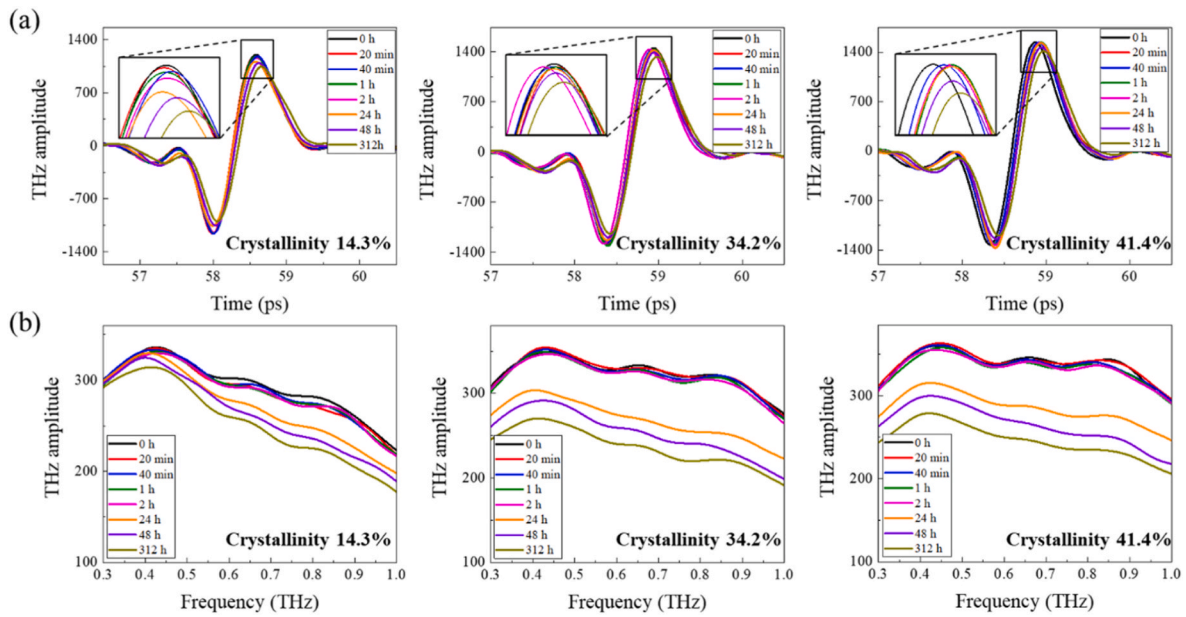
Fig. 7. Schematic representation of the THz signal according to the immersion time with different crystallinity: (a) THz time-domain signal of the PET specimen with 14.3, 34.2, and 41.4% crystallinity, and (b) THz frequency-domain signal of the PET specimen with 14.3, 34.2, and 41.4% crystallinity.
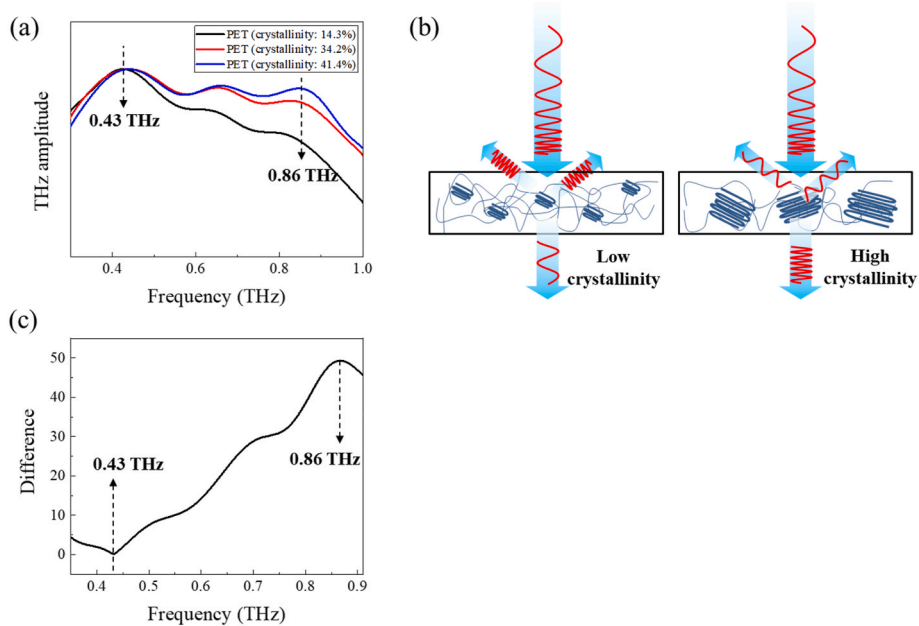

Fig. 8. Schematic representation of the THz wave according to the different crystallinity: (a) frequency-domain THz signal of dry PET specimens, (b) scattering mechanism of the PET specimen, and (c) THz amplitude differences according to the PET crystallinity.

3.2.2. Optical properties

For an in-depth study, the optical properties (refractive index and absorption coefficient) were analyzed to explain the behavior of the THz wave according to the crystallinity and moisture content of the PET specimens. The complex refractive index ($\tilde{n}_s$) was calculated with the refractive index (n_s) and extinction coefficient (k_s) of the specimen using Eq. (9):

$$\tilde{n}_s(\omega) = n_s(\omega) - i k_s(\omega) \tag{9}$$

The refractive index (n_s) and extinction coefficient (k_s) are described by the angular frequency (ω), phase difference ($\varnothing(\omega)$) between the reference signal (transmitted air) and the sample signal (transmitted specimen), speed of light (c), thickness of the specimen (d), refractive

index of air (n_{air}), and the magnitude ratio of the reference signal to the sample signal in the frequency-domain ($\rho(\omega)$) as shown in Eq. (10) and Eq. (11):

$$n_s(\omega) = \varnothing(\omega) \times \frac{c}{\omega \bullet d} + n_{air} \tag{10}$$

$$k_s(\omega) = \ln\left(\frac{4 n_s(\omega)}{\rho(\omega) \bullet (n_s(\omega) + 1)^2}\right) \times \frac{c}{\omega \bullet d} \tag{11}$$

The phase difference ($\varnothing(\omega)$) and magnitude ratio ($\rho(\omega)$) were obtained from the frequency-domain waveform with phase unwrapping [31]. In addition, the absorption coefficient (a_s) was calculated by the extinction coefficient (k_s) as shown in Eq. (12):
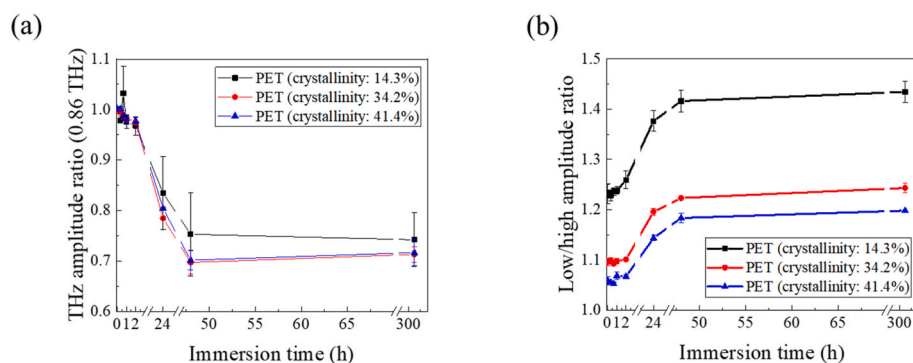
Fig. 9. Schematic representation of the THz wave parameters according to the crystallinity and immersion time: (a) THz amplitude ratio at 0.86 THz, and (b) low/high amplitude ratio.

$$a_s(\omega) = \frac{2\omega \bullet k_s}{c} \tag{12}$$

The optical properties of the PET specimens were analyzed at a frequency of 0.86 THz, which was sensitive to moisture along with crystallinity, as shown in Figs. 10 and 11. Using Eq. (10), the refractive index of the PET specimens was calculated (Fig. 10). The refractive index of the THz wave at the 0.86 THz frequency increased rapidly during the initial immersion period because the dielectric relaxation of water in the THz wave increased. Saturation was achieved after 2 h of immersion (Fig. 10-(a)). The refractive index increased more rapidly than the moisture content of the PET specimens because the refraction of the THz waves by water was dominant from the initial state of immersion (Fig. 10-(b)). In addition, the refractive index of the THz waves increased as the PET specimen crystallinity increased due to an increase in density [32].

The absorption coefficient of the PET specimens was derived using Eq. (11). The absorption coefficient increased with a decrease in crystallinity of the PET specimens (Fig. 11-(a)) because THz electromagnetic wave scattering increased due to the irregular polymer structure in the amorphous region [26]. The absorption coefficient also increased with immersion time as the THz waves were absorbed by water molecules in the specimens (Fig. 11-(a)). During the initial state of moisture absorption, the moisture content rate increased faster than that of the absorption coefficient. This may have been due to uneven moisture distribution across the entire specimen. After two days of immersion, the absorption coefficient gradually increased due to hydrolytic degradation of the PET polymer chains. It also has been previously reported that chemi-crystallization proceeded during immersion and the mobility of the macromolecules increased due to hydrolysis (Fig. 11-(b)) [33].

3.3. In-situ monitoring of PET crystallinity and moisture content using THz wave parameters

To simultaneously inspect the crystallinity and moisture content of the PET specimens, THz wave parameters (THz amplitude ratio and low/high amplitude ratio) were plotted with respect to absorbed moisture within the PET specimens (Fig. 12). The inverse THz amplitude ratio increased until the immersion duration reached 2 days and showed a similar tendency to that of the moisture content with different degrees of crystallinity. However, crystallinity was difficult to distinguish from moisture absorption by the THz amplitude ratio due to the influence of water molecules in the PET specimens. Fig. 12-(b) shows a plot of low/high amplitude ratio in a different region according to crystallinity. The low/high amplitude ratio showed a clear difference according to crystallinity of the PET specimens over all immersion periods; however, with the inverse THz amplitude ratio, the graph overlapped at 41.4% and 34.2% crystallinity over the entire immersion period (see Fig. 12-(a)).

The THz parameters were plotted again according to the moisture content and crystallinity of the PET specimens (Fig. 13). As shown in Fig. 13-(a), the inverse THz amplitude ratio was sensitive to moisture absorption rather than specimen crystallinity. Especially at the onset of moisture absorption, the plots of the inverse THz ratio overlapped, hindering classification of PET specimen crystallinity. Meanwhile, the low/high amplitude ratio changed linearly due to the crystallinity of the PET specimens over the entire moisture absorption range but did not change as much as the inverse THz ratio due to the moisture content of the PET specimens (Fig. 13-(b)). Therefore, in this work, we proposed a new THz inspection algorithm to simultaneously monitor and distinguish the crystallinity and moisture content of PET specimens using low/high amplitude and inverse THz amplitude ratios as shown in Fig. 14. To simultaneously examine the crystallinity and moisture content of the PET specimens, the low/high amplitude and inverse THz
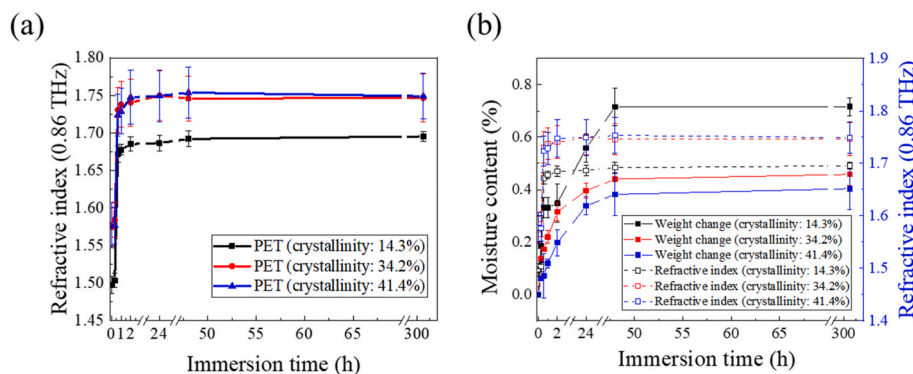

Fig. 10. Refractive index of the PET specimen during the moisture absorption according to the different crystallinity: (a) at 0.86 THz, and (b) comparison with moisture content.
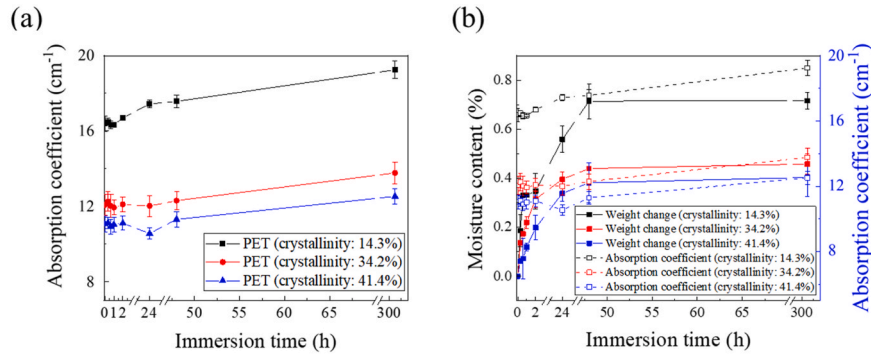
Fig. 11. Absorption coefficient of the PET specimen during the moisture absorption according to the different crystallinity: (a) at 0.86 THz, and (b) comparison with moisture content.
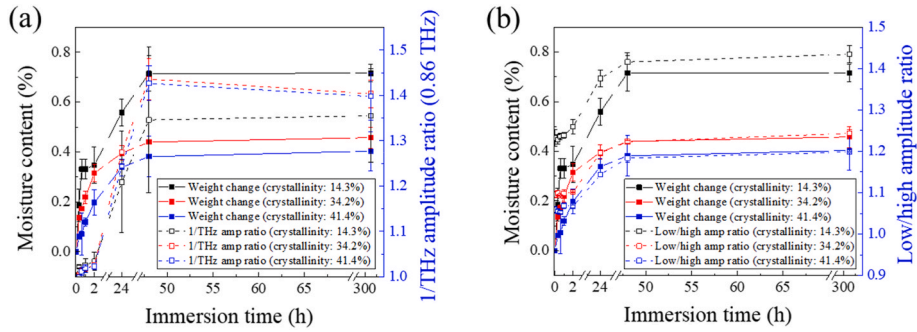

Fig. 12. The comparison of the moisture content and THz wave parameters of the PET specimen: (a) invers THz amplitude ratio at 0.86 THz, and (b) low/high amplitude ratio.
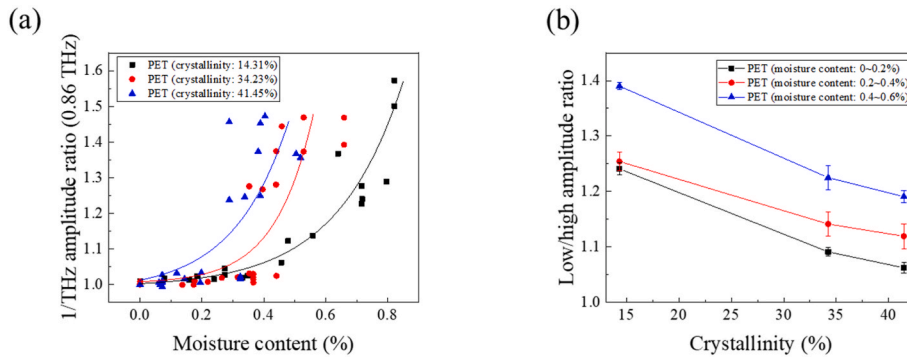

Fig. 13. The comparison of the THz wave parameters and PET specimen properties: (a) invers THz amplitude ratio at 0.86 THz, and (b) low/high amplitude ratio.

amplitude ratios of the PET specimens with different moisture and crystallinity levels were co-plotted as shown in Fig. 14. Both THz wave parameters increased with increase in moisture absorption, though they increased at different slopes. No curve overlapped according to crystallinity or moisture content. Based on the study, the co-plot graph was extended to the THz wave parameter map (Fig. 15) generated by extrapolating the curves of Fig. 14 using linear regression analysis with respect to crystallinity and moisture content (using Eq. (13)). The regression parameters of slope (*m*) and intercept (*b*) were determined using the least squares method (LSM) and were defined by Eqs. (14) and (15), respectively:

$$y = mx + b \tag{13}$$

$$m = \frac{\sum\limits_{i=1}^{n}(x_i - \bar{x})(y_i - \bar{y})}{\sum\limits_{i=1}^{n}(x_i - \bar{x})^2} \tag{14}$$

$$b = \bar{y} - m\bar{x} \tag{15}$$

where x_i, $\bar{x}$, y_i, y, *and* n are the crystallinity, average crystallinity, THz wave parameters, average of the THz wave parameters, and number of specimens, respectively. The correlation between the THz wave parameters in the regression model (Table 2) can be expressed as Eq. (16) using the THz map coefficient (z). Therefore, the crystallinity and moisture content of PET can be measured through the THz wave parameter position of the specimen in Fig. 15, which can be expressed as Eqs. (17) and (18).
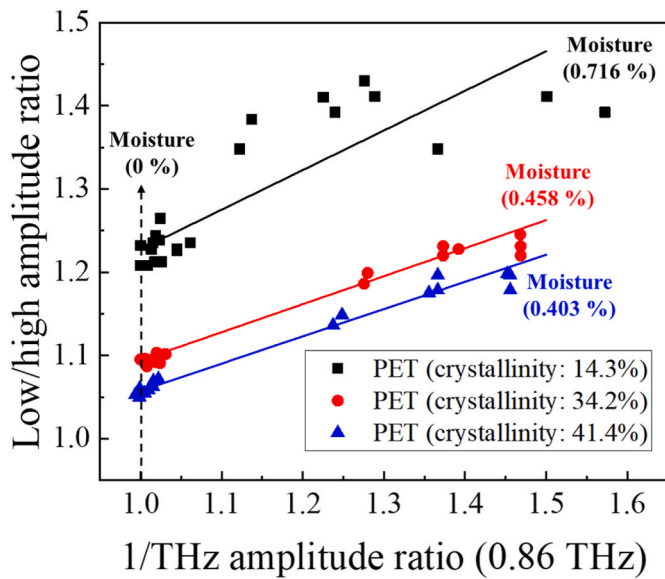
Fig. 14. Schematic representation of the THz wave parameters curve according to the different crystallinity and moisture content PET specimens.
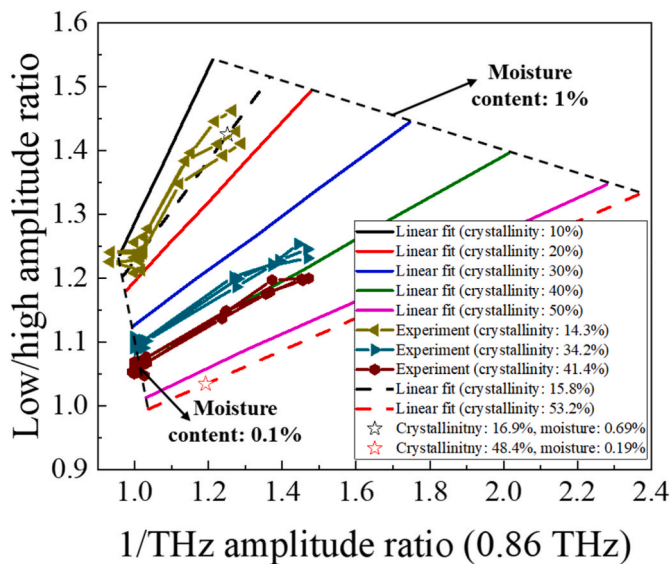

Fig. 15. Schematic representation of the THz wave parameter map considering the moisture content and crystallinity of the PET specimen.

$$\widetilde{E}_{low\;to\;high} = \frac{122.9 + 0.0281 \bullet z}{(101.2 + z) \bullet \widetilde{E}_{amp\;ratio}} + \frac{7.20 + 1.13 \bullet z - 0.000565 \bullet z^2}{101.2 + z} \quad (16)$$

$$Crystallinity = \frac{(0.959 + 0.00018 \bullet z) - 0.959}{1.031 - 0.959} \times 40 + 10 \quad (17)$$

$$Moisture\;content = \frac{1/\widetilde{E}_{amp\;ratio} - (0.959 + 0.00018 \bullet z)}{0.00249 \bullet z + 0.252} \times 0.9 + 0.1 \quad (18)$$

The THz wave parameters of the test specimens were used to evaluate the accuracy of the proposed THz wave parameter map (Fig. 15). By comparing the predicted PET properties with the actual properties measured via DSC and gravimetric measurement methods, it was confirmed that the THz wave parameter map predicted the properties of the PET specimens within a 10% error margin (Table 3). Consequently, the crystallinity and moisture content of the PET specimens were successfully monitored simultaneously by the THz wave parameters measured during one-time THz monitoring. However, the limited number of gradients (three) in the current LSM approach may not provide a standardized measurement of crystallinity in PET specimens. Nonetheless, these findings demonstrate the potential for simultaneous inspection of polymer crystallinity and moisture content using THz technology, indicating its promising applicability to polymer products.

4. Conclusions

The degree of crystallinity and moisture content of the PET specimens were simultaneously inspected using a THz-TDS system. By analyzing the THz signal with crystallinity and moisture content, relationships between THz wave properties (THz amplitude ratio, low/high amplitude ratio, refractive index, and absorption coefficient) and PET properties (degree of crystallinity and moisture content) were discovered. In addition, the THz wave properties were compared with conventional methods for verification. DSC and XRD confirmed that the crystallite size of the PET specimens was affected by the degree of crystallinity. The THz scattering frequency region shifted depending on crystallite size, and the degree of crystallinity influenced the THz wave properties. Furthermore, since water molecules influenced the signal over the entire THz bandwidth, the THz properties correlated with the crystallinity and moisture content of the PET specimens. Consequently, using the THz wave parameters, the degree of crystallinity and moisture content of the PET specimens could be monitored simultaneously.

The technique developed in this research can be used as a multipurpose inspection method to universally examine properties such as crystallinity and moisture content of non-metallic materials. In particular, it can be applied for real-time inspection of polymer products used in electronic components susceptible to crystallinity and external moisture, such as EMC (Epoxy molding compound), semiconductor packaging materials, and solar panel substrates. However, this method has limitations when inspecting materials containing metals or thick products that cannot be transmitted by terahertz waves. Overall, this terahertz wave-based system has the potential to be widely used as an inline process monitoring technology for non-destructively inspecting the crystallinity and moisture content of polymer products. Consequently, this research technique can contribute to the development of a new approach to non-destructive testing of polymer materials using

Table 2
The regression parameters of the invers THz amplitude ratio and low/high amplitude ratio models.

Moisture content [%]	1/THz amplitude ratio		Low/high amplitude ratio	
	Slop	Bias	Slop	Bias
0.1	0.0018	0.9414	−0.0056	1.2925
0.3	0.0073	0.9420	−0.0054	1.3590
0.5	0.0129	0.9427	−0.0053	1.4254
0.7	0.0184	0.9434	−0.0051	1.4919
1	0.0267	0.9444	−0.0049	1.5916

Table 3
Comparison between the predicted PET properties by the THz wave parameter map and the measured PET properties by the conventional methods.

Test specimen	Crystallinity [%]			Moisture content [%]		
	Actual	Predicted	Error [%]	Actual	Predicted	Error [%]
1	16.9	15.8	6.7	0.69	0.74	7.44
2	48.4	53.2	9.9	0.19	0.21	9.27

terahertz waves.

Credit author statement

Sang-Il Kim: Conceptualization, Methodology, Writing - Original Draft, Investigation.
Dong-Woon Park: Formal analysis, Resources, Validation.
Heon-Su Kim: Writing - Review & Editing, Resources, Methodology.
Hak-Sung Kim: Supervision, Project administration, Conceptualization.

Declaration of competing interest

The authors declare that they have no known competing financial interests or personal relationships that could have appeared to influence the work reported in this paper.

Data availability

The raw/processed data required to reproduce these findings cannot be shared at this time due to technical or time limitations.

Acknowledgements

Appendix A. Supplementary data

Supplementary data to this article can be found online at https://doi.org/10.1016/j.polymertesting.2023.108085.

References

[1] K. Gotoh, A. Yasukawa, Y. Kobayashi, Wettability characteristics of poly (ethylene terephthalate) films treated by atmospheric pressure plasma and ultraviolet excimer light, Polymer J. 43 (2011), https://doi.org/10.1038/pj.2011.20, 545-551.

[2] R. Nisticò, Polyethylene terephthalate (PET) in the packaging industry, Polymer Test. 106707 (2020), https://doi.org/10.1016/j.polymertesting.2020.106707.

[3] S.B. Kim, N.H. Yi, H.Y. Kim, J.-H.J. Kim, Y.-C. Song, Material and structural performance evaluation of recycled PET fiber reinforced concrete, Cement Concr. Compos. 32 (2010) 232–240, https://doi.org/10.1016/j.cemconcomp.2009.11.002.

[4] S.G. Hashmi, et al., A durable SWCNT/PET polymer foil based metal free counter electrode for flexible dye-sensitized solar cells, 2, https://doi.org/10.1039/C4TA03730H, 2014, 19609–19615.

[5] B. Demirel, A. Yaraş, H. Elçiçek, Crystallization behavior of PET materials. http://hdl.handle.net/11772/1592, 2011.

[6] S.A. Jabarin, E.A. Lofgren, Effects of water absorption on physical properties and degree of molecular orientation of poly (ethylene terephthalate), Polymer Eng. Sci. 26 (1986) 620–625, https://doi.org/10.1002/pen.760260907.

[7] Ahmad, Mohammad Asraf Alif, et al., Dynamic mechanical analysis and effects of moisture on mechanical properties of interwoven hemp/polyethylene terephthalate (PET) hybrid composites, Construct. Build. Mater. 179 (2018) 265–276, https://doi.org/10.1016/j.conbuildmat.2018.05.227.

[8] T. Sang, C.J. Wallis, G. Hill, G.J. Britovsek, Polyethylene terephthalate degradation under natural and accelerated weathering conditions, Eur. Polymer J. 109873 (2020), https://doi.org/10.1016/j.eurpolymj.2020.109873.

[9] Y. Kong, J. Hay, The measurement of the degree of crystallinity of polymers by DSC, 66(2006) 379–386, Polymer 43 (2002) 3873–3878, https://doi.org/10.1016/S0032-3861(02)00235-5.

[10] H.-J. Um, Y.-T. Hwang, K.-H. Choi, H.-S. Kim, Effect of degree of crystallinity on the mechanical behavior of carbon fiber reinforced polyethylene-terephthalate (CF/PET) composites considering temperature conditions, Compos. Sci. Technol. 207 (2021) 108745, https://doi.org/10.1016/j.compscitech.2021.108745.

[11] Sandeep Tamrakar, Roberto A. Lopez-Anido, Water absorption of wood polypropylene composite sheet piles and its influence on mechanical properties, Construct. Build. Mater. 25.10 (2011) 3977–3988, https://doi.org/10.1016/j.conbuildmat.2011.04.031.

[12] W. Wang, M. Sain *, P.A. Cooper. Study of moisture absorption in natural fiber plastic composites. Compos. Sci. Technol.. https://doi.org/10.1016/j.compscitech.2005.07.027.

[13] Babak Kateb, et al., Infrared thermal imaging: a review of the literature and case report, Neuroimage 47 (2009) T154–T162, https://doi.org/10.1016/j.neuroimage.2009.03.043.

[14] Prasad, Balla Srinivasa, K. Aruna Prabha, P.V.S. Ganesh Kumar, Condition monitoring of turning process using infrared thermography technique–An experimental approach, Infrared Phys. Technol. 81 (2017) 137–147, https://doi.org/10.1016/j.infrared.2016.12.023.

[15] Yajian Wang, Pengpeng Li, Jianfeng Li, The monitoring approaches and non-destructive testing technologies for sewer pipelines, Water Science and Technology 85 (10) (2022), https://doi.org/10.2166/wst.2022.120, 3107–3121.

[16] Yong-Kai Zhu, et al., A review of optical NDT technologies, Sensors 11.8 (2011) 7773–7798, https://doi.org/10.3390/s110807773.

[17] Shuncong Zhong, Progress in terahertz nondestructive testing: a review, Front. Mech. Eng. 14 (2019) 273–281, https://doi.org/10.1007/s11465-018-0495-9.

[18] Dirk Nüßler, Joachim Jonuscheit, Terahertz based non-destructive testing (NDT), TM - Tech. Mess. 88.4 (2021) 199–210, https://doi.org/10.1515/teme-2019-0100.

[19] Stefan Sommer, et al., THz-spectroscopy on high density polyethylene with different crystallinity, J. Infrared, Millim. Terahertz Waves 37 (2016) 189–197, https://doi.org/10.1007/s10762-015-0219-8.

[20] Han Wang, Satoru Tsuchikawa, Tetsuya Inagaki, Terahertz time-domain spectroscopy as a novel tool for crystallographic analysis in cellulose: the potentiality of being a new standard for evaluating crystallinity, Cellulose 28.9 (2021) 5293–5304, https://doi.org/10.1007/s10570-021-03902-x.

[21] Vieira, Francisco Senna, Celio Pasquini, Determination of cellulose crystallinity by terahertz-time domain spectroscopy, Anal. Chem. 86.8 (2014) 3780–3786, https://doi.org/10.1021/ac4035746.

[22] Shusaku Nakajima, et al., Determination of starch crystallinity with the Fourier-transform terahertz spectrometer, Carbohydr. Polymers 262 (2021) 117928, https://doi.org/10.1016/j.carbpol.2021.117928.

[23] M. Stecher, et al., Towards industrial inspection with THz systems, in: Ultrashort Pulse Laser Technology, Springer, 2016, https://doi.org/10.1007/978-3-319-17659-8_14.

[24] I. Amenabar, F. Lopez, A. Mendikute, In introductory review to THz non-destructive testing of composite mater, J. Infrared, Millim. Terahertz Waves 34 (2013) 152–169, https://doi.org/10.1007/s10762-012-9949-z.

[25] C. Rønne, P.-O. Åstrand, S.R. Keiding, THz spectroscopy of liquid H 2 O and D 2 O, Phys. Rev. Lett. 82 (1999) 2888, https://doi.org/10.1103/PhysRevLett.82.2888.

[26] R.B. Richards, Polyethylene-structure, degree of crystallinity and properties, J. Appl. Chem. 1.8 (1951) 370–376, https://doi.org/10.1002/jctb.5010010812.

[27] S. Lasoski Jr., W. Cobbs Jr., Moisture permeability of polymers. I. Role of degree of crystallinity and orientation, J. Polymer Sci. 36 (1959) 21–33, https://doi.org/10.1002/pol.1959.1203613003.

[28] Do-Hyoung Kim, et al., Nondestructive evaluation of hidden damages in glass fiber reinforced plastic by using the terahertz spectroscopy, Int. J. Precis. Eng. Manuf.-Green Technol. 4.2 (2017) 211–219, https://doi.org/10.1007/s40684-017-0026-x.

[29] X. Xin, et al., Terahertz absorption spectrum of para and ortho water vapors at different humidities at room temperature, J. Appl. Phys. 100.9 (2006), 094905, https://doi.org/10.1063/1.2357412.

[30] Suk-Ho Hong, Jörg Winter, Size dependence of optical properties and internal structure of plasma grown carbonaceous nanoparticles studied by in situ Rayleigh-Mie scattering ellipsometry, J. Appl. Phys. 100.6 (2006), 064303, https://doi.org/10.1063/1.2338132.

[31] Heon-Su Kim, et al., Non-destructive evaluation of cement hydration with pulsed and continuous Terahertz electro-magnetic waves, Optics and Lasers Eng. 138 (2021) 106414, https://doi.org/10.1016/j.optlaseng.2020.106414.

[32] D.E. Bosley, X-ray determination of crystallinity in poly (ethylene terephthalate), J. Appl. Polym. Sci. 8.4 (1964) 1521–1529, https://doi.org/10.1002/app.1964.070080402.

[33] Mael Arhant, et al., Impact of hydrolytic degradation on mechanical properties of PET-Towards an understanding of microplastics formation, Polym. Degrad. Stabil. 161 (2019) 175–182, https://doi.org/10.1016/j.polymdegradstab.2019.01.021.